ENSO control on the South Asian Monsoon through the length of the rainy season

B. N. Goswami and Prince K. Xavier

Centre for Atmospheric and Oceanic Sciences, Indian Institute of Science, Bangalore, 560012, INDIA

Abstract. Being an integral effect of sub-seasonal rain spells over the season, the seasonal mean south Asian monsoon (SAM) rainfall could be affected by change in the length of the rainy season (LRS). An objective definition of the duration of the SAM season has, however, been lacking. Here we show that the meridional gradient of tropospheric temperature (ΔTT) over the SAM region controls the LRS and defines the SAM season. It is further shown that ENSO induces decreased SAM rainfall by regulating the LRS. The atmospheric response to tropical sea surface temperature (SST) over the tropical Pacific during an evolving El Niño reduces ΔTT over the SAM region and shortens LRS by delaying the onset and advancing the withdrawal. The strong negative correlation between LRS and ENSO related SST has remained steady and provides basis for improved prediction of seasonal mean SAM rainfall variability.

1. Introduction

Based on spatial coherence of seasonal rainfall, the south Asian monsoon (SAM) region includes parts of Arabian Sea, the Indian continent and the north Bay of Bengal [*Goswami et al.,* 1999]. The inverse relationship between ENSO and the SAM rainfall has so far been linked to modification of large-scale environment for organized convection associated with the eastward shift of the Walker circulation [*Webster et al.,* 1998; *Kumar et al.,* 1999; *Krishnamurthy and Goswami,* 2000; *Lau and Nath,* 2000]. The seasonal mean rainfall can also be influenced by significant change in the length of the rainy season (LRS). The conventional definition of the SAM season to be between June 1 and September 30 is arbitrary but an objective definition of exact SAM season has been lacking. The primary character of the SAM being sustained enhanced precipitation on continental scale, the monsoon 'onset' over Kerala (MOK) and 'withdrawal' from the southern tip of the continent (around 10°N) delineates the SAM season. In some years, SAM 'onset' takes place significantly earlier than June 1 while 'withdrawal' can take place weeks after September 30. Non-inclusion of rain spells outside the traditional definition of the SAM season may significantly influence the interannual variability (IAV) of the seasonal mean SAM rainfall and its teleconnection with other global phenomena such as the El Niño and Southern Oscillation (ENSO). Here we identify the physical process that controls the 'onset' and 'withdrawal' of the SAM and provide an objective method for the age-old problem of defining the SAM season. This new definition also helps us to unravel a mechanism, not recognized so far, through which ENSO influences the SAM rainfall.

Paper number .
0094-8276/05/$5.00

2. Onset, Withdrawal and LRS of SAM: Physical basis

Large poleward shift of the rain belt (tropical convergence zone, TCZ) over the SAM region during northern summer [*Gadgil,* 2003] is a manifestation of repeated northward migration of the TCZ from near the equator to about 25°N on intraseasonal time scale [*Goswami,* 2005]. MOK represents the beginning of large scale organized deep convection with rather abrupt transition from dry to wet condition [*Soman and KrishnaKumar,* 1993] and sets up the large-scale background condition for northward propagation of the TCZ. The SAM season ends or 'withdraws' from the continental region when the large-scale conditions inhibit northward propagation of the TCZ north of 10°N. Actual dates of these two events are governed by the change in sign of the meridional gradient of the tropospheric non-adiabatic heating over the region, effectively represented by the tropospheric temperature averaged between 200 hPa and 700 hPa (TT). The climatological mean difference in TT (ΔTT) averaged over the north and south boxes (Fig.1,inset) calculated from NCEP/NCAR reanalysis [*Kalnay et al.,* 1996] (hereafter referred to as NC) is shown in Fig.1. We define the onset (withdrawal) of the SAM as the date when the ΔTT changes from negative to positive (positive to negative). The two boxes are chosen such that the ΔTT represents the large scale heating gradients driving the large scale SAM circulation reasonably well. While some form of change of sign of ΔTT has been associated with monsoon onset earlier [*Li and Yanai,* 1996; *He et al.,* 2003], here we propose that it is also associated with the withdrawal and provide a physical basis for the same (see below).

The classical land-ocean contrast model involving surface temperature gradient forces only a shallow circulation [*Schneider and Lindzen,* 1977] and cannot explain the deep vertical structure of the SAM . The meridional gradient of deep tropospheric heating is primarily responsible for the deep SAM circulation and may be effectively represented by the meridional gradient of TT [*Webster et al.,* 1998]. Sensible heating over the Tibetan Plateau during the pre-monsoon period plays a crucial role in setting up the deep heating in the northern location [*Yanai et al.,* 1992; *Li and Yanai,* 1996] and is instrumental in reversing the meridional gradient of TT. After the SAM onset, latent heat released from SAM precipitation contributes significantly to the northern heat source. In addition, heat advection associated with quasi-stationary planetary waves can also

influence the temperature of the northern part and hence the meridional gradient of TT. Land surface heating (heat low) during late April and May produces surface convergence (north of 10°N) of warm moist air from south but is capped by a subsidence and southward flow of drier colder air above the planetary boundary layer (PBL). The process builds up potential convective instability to a high level but could not be realized due to the inhibition of subsidence above the PBL. The change in the sign of meridional gradient of TT ushers in the off-equatorial large-scale deep heat source. The atmospheric response to such a heat source

Table 1. Statistics of onset date (OD), withdrawal date (WD) and length of the rainy season (LRS) from NC and ERA (in Julian days).

	Mean NC (ERA)	S.D. NC (ERA)
OD	149 (145)	6.5 (6.6)
WD	278 (279)	7.2 (7.4)
LRS	129 (133)	10.6 (11.1)

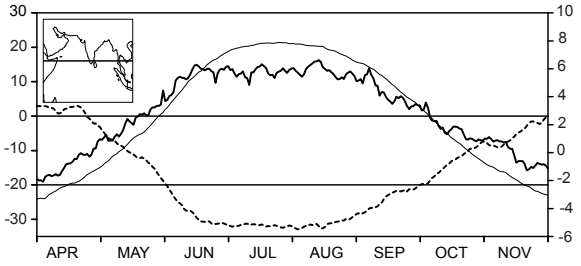

Figure 1. ΔTT between the two boxes (thin solid, K × 6, the zonal extent of both boxes is between 30° - 110°E while the merdional extent of the northern (southern) box is between 10°N - 35°N (15°S - 10°N), shown in inset), vertical shear of zonal wind (200 hPa - 850 hPa) averaged over 50°E-90°E, Eq.-15°N (dashed, m s^{-1}) and latitude of zero absolute vorticity averaged between 50°E and 100°E (thick solid, right scale).

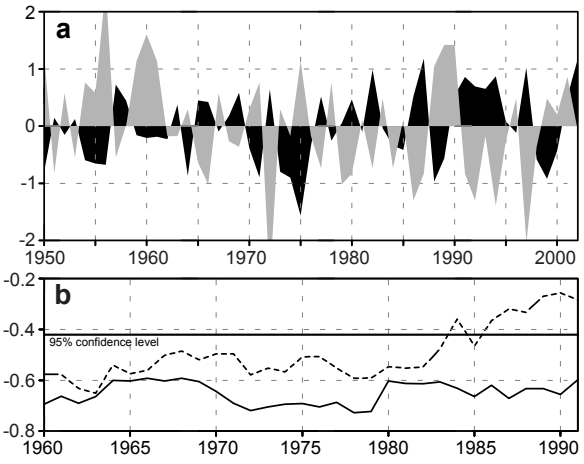

Figure 2. (a) Time series of normalized anomaly of LRS (grey) and Niño4 SST (black). (b) 21-year moving window correlation between JJAS AIR and Niño4 SST (dashed) and between LRS and Niño4 SST (solid).

Table 2. Correlation between OD, WD and LRS, and other parameters. EIMR (see text) is from NC precipitaton.

	MOK	AIR (MJJASO)	EIMR (LRS)	EIMR (JJAS)	Niño3 (JJAS)	Niño4 (JJAS)
OD	0.64[b]	-0.36[a]	-0.56[b]	-0.15	0.46[b]	0.47[a]
WD	-0.2	0.64[b]	0.62[b]	0.21	-0.47[b]	-0.54[b]
LRS	-0.51[b]	0.64[b]	0.75[b]	0.24	-0.59[b]	-0.63[b]

[a] Significant at 5% level; [b] significant at 1% level

[*Gill,* 1980; *Rodwell and Hoskins,* 1996] leads to cross equatorial flow and large scale cyclonic circulation above the planetary boundary layer (PBL). This moves the zero absolute vorticity line at 850 hPa to north of the equator [*Tomas and Webster,* 1997] (about 5°N, Fig.1, thick solid) and facilitates triggering symmetric inertial instability. The symmetric instability [*Tomas and Webster,* 1997; *Krishnakumar and Lau,* 1998] overcomes the inhibition by forcing frictional boundary layer convergence and leads to explosive development of off-equatorial organized convection (namely TCZ)

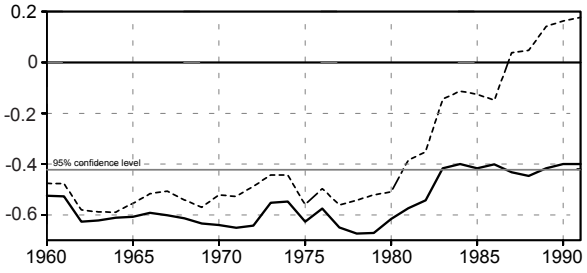

Figure 3. 21-year moving window correlation between JJAS EIMR and Niño4 SST (dashed) and between LRS EIMR and Niño4 SST (solid).

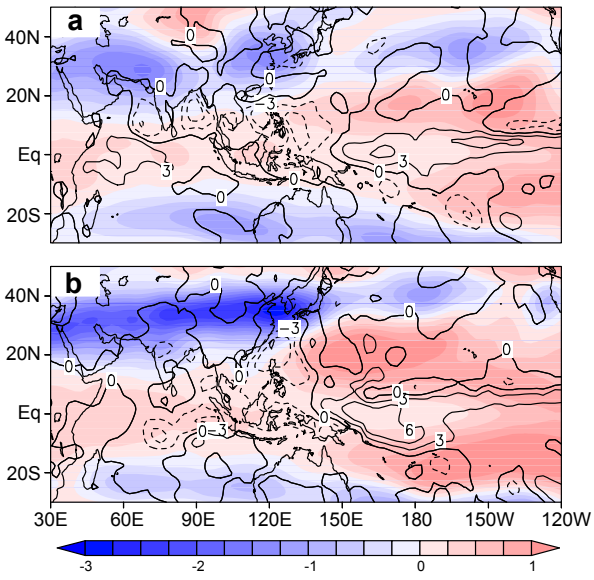

Figure 4. El Niño minus La Nina composites of TT (shaded, K) and rainfall (contours, mm day^{-1}) anomalies averaged between (a) 15 May and 15 June and (b) 15 September and 15 October. Composites are based on 8 El Niño years (1957,65,72,79,82,87,92 and 97) and 7 La Nina years (1955,64,70,73,75,88 and 99) defined using normalized Niño4 SST anomalies being > 1 (< -1).

and 'onset' of SAM (i.e., MOK). Progression further north and maintenance of SAM depends on the poleward propagation of the TCZ, which, in turn, depends crucially on the easterly vertical shear of the mean zonal wind [*Jiang et al.,* 2004]. The critical value of easterly shear of mean zonal wind between 200 and 850 hPa averaged over 50°E-90°E,Eq.-15°N (from NC) required for sustained northward propagation appears to be around 20 m s^{-1} (Fig.1, dashed). Lesser poleward extent of the seasonal mean precipitation band and weaker poleward propagation of the TCZ over the east-Asian monsoon (between 110°E-150°E) is due to a combination of weaker ΔTT and weaker easterly shear of the mean zonal wind (see Supplementary Fig.1). Thus, MOK and withdrawal defined in this manner are physically based and does not require an ad-hoc magic threshold of precipitation as in most traditional definitions. While rainfall based withdrawal date (WD) of south-west monsoon from Kerala could be ambiguous due to rainfall from north-east monsoon, our definition WD is an unambiguous end of the south-west monsoon season as it indicates time of transition from a heat source north of 10°N to one located south of 10°N and that the northward propagation of TCZ north of 10°N ceases after this date. Being based on averages over a large region, our onset date (OD) is also less sensitive to small-scale processes and less susceptible for 'bogus' onsets.

Statistics of the onset (OD) and withdrawal (WD) dates and length of the rainy season (LRS = WD-OD) obtained from NC between 1950 and 2003 shows (Table-1) that the mean onset (29 May) and withdrawal (5 October) dates are close to the climatological MOK [*Soman and KrishnaKumar,* 1993] and withdrawal dates obtained from traditional methods. The mean LRS is about 7 days longer than the traditionally used June-September monsoon season and its variability is much larger than that of either OD or WD. Mean and standard deviation (S.D) of OD, WD and LRS obtained from ERA-40 [*Uppala et al.,* 2004], based on period between 1958 and 2002 are very similar to those obtained from NC (Table-1). The definition of OD, WD and LRS in this manner is rather robust as evident from strong correlation between them obtained from NC and ERA-40 (being 0.70, 0.98 and 0.89 respectively). Most discrepency between the two data sets appears in OD. We find that ERA is little more sensitive to bogus onsets. While OD is almost idential in both data sets for 38 of the 45 common years, ERA gives systematically early (bogus) OD in seven years (see supplimentary Fig.2 and supplimentary Table-2). Due to longer data length and more stable OD (and hence LRS), all subsequent analysis is based on NC. To remove influence of known decadal climate shift around mid 1970's in NC and SST, the weak trend in OD, WD, LRS and SST has been removed.

The OD obtained by our method correlates well with the MOK from India Meteorological Department [*Joseph et al.,* 1994] (Table-2). This is consistent with our hypothesis that the thermodynamic definition of OD should be related with the precipitation based definition (e.g.MOK) through mechanisms discussed earlier in this section. The extremes of LRS differ by 46 days, much larger than those for either OD or WD (30 days). Such changes in LRS can affect the seasonal mean SAM rainfall simply by embracing more or curtailing the number of sub-seasonal rain spells. Influence of LRS on seasonal mean monsoon rainfall is evident from its significant strong correlation of LRS with May-October all India rainfall (AIR [*Parthasarathy et al.,* 1994])(Table-2). While OD is positively correlated and WD negatively, the LRS is strongly negatively correlated with Niño3 SST or Niño4 SST. Coherent interannual variation of Niño4 SST and LRS anomalies is evident from their normalized time series (Fig.2a). Unlike the correlation between the June-September AIR with Niño4 SST that decreases to insignificant values during the recent decades (Fig.2b, dashed), the correlation between LRS and Niño4 SST has remained robust and highly significant throughout the period (Fig.2b, solid). As daily AIR for the period is not currently available, it is not possible to examine similar correlations of JJAS AIR and AIR for LRS periods with Niño4 SST. In the absence of such data, we calculate extended Indian monsoon rainfall, EIMR [*Goswami et al.,* 1999] for JJAS and LRS periods from NCEP reanalysis precipitation. Dramatic difference between 21-year sliding correlations between JJAS EIMR and LRS EIMR is noteworthy (Fig.3). Stability of the correlations between LRS EIMR and Niño4 SST indicates that a part of the so called weakening of ENSO-monsoon relationship [*Kumar et al.,* 1999; *Krishnamurthy and Goswami,* 2000] during recent decades may be simply due to not defining the monsoon season correctly.

3. ENSO regulation of LRS (SAM): Mechanism

The correlation map of JJAS SST and LRS (see Supplementary Fig.3) shows that the large scale ENSO related SST pattern is closely linked with the LRS variability. The slow evolution of ENSO SST has a clear and definite influence on OD, WD and LRS as the sign of correlation between all three parameters with Niño4 SST of each month from January till December remains same (see supplimentary Table-1).

ENSO regulates LRS through the atmospheric response to the diabatic heating associated with the ENSO SST that leads to a substantial reduction of the meridional gradient of TT over the SAM region during May and September. The El Niño minus La Nina composite TT anomalies averaged between 15 April -15 May and 15 September - 15 October (Fig.4) illustrates that the withdrawal phase is more strongly influenced by the ENSO SST compared to the onset phase. Further, most of the reduction (increase) in TT during El Niño (La Nina) occurs over the northern box between 10°N and 35°N. The spatial pattern of ENSO induced TT anomalies is consistent with response of tropical atmosphere to ENSO SST induced diabatic heating (see supplimentary Fig.5) through tropical wave dynamics [*Rodwell and Hoskins,* 1996; *Hui et al.,* 2003]. Although, the SAM region is far away from the core convection associated with the ENSO, the tropical wave dynamics provides an atmospheric bridge that helps ENSO regulate the LRS by modulating the ΔTT. El Niño and La Nina composites of vertical shear (between 200 hPa and 850 hPa) of zonal winds averaged between 50°E-90°E, Eq.-15°N and ΔTT (see supplimentary Fig.4) show that the critical strength of the wind shear (about -20 m s^{-1}) is reached about 10 days later during onset phase and weaken below the critical strength about 15 days earlier during withdrawal phase in El Niño years compared to La Nina years. On the average, during El Niño years this leads to a delay of the onset by about 9 days and an advancement of the withdrawal by about 10 days compared to La Nina years (see supplimentary Fig.5).

4. Conclusions and discussions

An objective method for the age-old problem of defining the SAM season is proposed. Accordingly, the period between 15 May and 15 October may be considered as the SAM season to take into account southwest monsoon rains outside the traditional 1 June - 30 Sepetmber definition. Interannual variability of SAM rainfall with this definition of the season should be reconstructed and all teleconnections re-examined.

A mechanism, not recognized so far, is discovered where ENSO controls SAM rainfall by controling the LRS. Through atmospheric response of SST induced diabatic heating, El Niño (La Niña) weakens (stengthens) ΔTT over the SAM region and shortens (lengthens) LRS and SAM rainfall. This mechanism is different but not inconsistent with the ENSO influence on SAM through change in Walker circulation. The weakening of zonal wind shear during El Niño's over the onset and withdrawal phases is indeed linked to the shift of the Walker circulation. We recall that the SAM rainfall could be affected by the LRS as well as level of activity of monsoon intraseasonal oscillations (ISOs) and its probability density function (PDF) within the season. The variability of SAM rainfall would depend entirely on the LRS if the ISO activity and its PDF within the season do not vary. However, the amplitude of ISO activity as well as its PDF could vary independent of the LRS due to internal dynamics of the atmosphere. In the recent years, the IAV of the seasonal mean SAM rainfall seems to be dominated by such internal IAV [*Goswami,* 2004]. Such internal IAV are not modulated by large-scale variability associated with ENSO and hence uncorrelated with it. In light of this, the weakening relationship between June-September all India rainfall (AIR) and ENSO indices [*Krishnamurthy and Goswami,* 2000; *Kumar et al.,* 1999] in contrast to the significant and steady relationship between LRS and ENSO indices may be reconciled. With the prediction of the ENSO six to nine months in advance becoming a reality, the steadiness of the ENSO - LRS relationship provides hope for better prediction of the ENSO forced component of SAM variability.

Acknowledgments. This work is partially supported by a grant from the Department of Ocean Development, New Delhi India. We thank Prof. D. Sengupta for comments, and Madhusoodanan M.S. and Feby Jose for help in preparing the manuscript.

References

Gadgil, S., The Indian Monsoon And Its Variability, *Annu.Rev.Earth Planet.Sci*, *31*, 429–467, 2003.

Gill, A. E., Some simple solutions for heat-induced tropical circulation, *Quart. J. Roy. Meteor. Soc.*, *106*, 447–462, 1980.

Goswami, B. N., Interdecadal change in potential predictability of the Indian summer monsoon, *Geophys. Res. Lett.*, *31*, doi:10.1029/2004GL020,337, 2004.

Goswami, B. N., South Asian Monsoon, in *Intraseasonal variability in the Atmosphere-Ocean climate system*, edited by K. Lau and D. Waliser, pp. 19–61, Praxis. Springer Berlin Heidelberg, 2005.

Goswami, B. N., V. Krishnamurthy, and H. Annamalai, A broad-scale circulation index for interannual variability of the Indian summer monsoon, *Quart. J. Roy. Meteor. Soc.*, *125*, 611–633, 1999.

He, H., C.-H. Sui, M. Jian, Z. Wen, and G. Lan, The evolution of tropospheric temperature field and its relationship with the onset of Asian summer monsoon, *J. Meteor. Soc. Japan*, *81*, 1201–1223, 2003.

Hui, S., D. Neelin, and J. E. Meyerson, Sensitivity of tropospheric temperature to see surface temperature forcing, *J. Climate*, *16*, 1283–1301, 2003.

Jiang, X., T. Li, and B. Wang, Structures and mechanisms of the northward propagation boreal summer intraseasonal oscillation, *J. Climate*, *17*, 1022–1039, 2004.

Joseph, P. V., J. Eischeid, and R. Pyle, Interannual variability of the onset of the Indian summer monsoon and its association with atmospheric features, El Niño and sea surface temperature anomalies, *J. Climate*, *7*, 81–105, 1994.

Kalnay, E., et al., The NCEP/NCAR 40-year reanalysis project, *Bull. Amer. Meteor. Soc.*, *77*, 437–471, 1996.

Krishnakumar, V., and K. M. Lau, Possible role of symmetric instability in the onset and abrupt transition of the Asian monsoon, *J. Meteor. Soc. Japan*, *76*, 363–383, 1998.

Krishnamurthy, V., and B. N. Goswami, Indian monsoon-ENSO relationship on inter decadal time scales, *J. Climate*, *13*, 579–595, 2000.

Kumar, K. K., B. Rajagopalan, and M. A. Cane, On the weakening relationship between the Indian Monsoon and ENSO, *Science*, *284*, 2156–2159, 1999.

Lau, N. C., and M. J. Nath, Impact of ENSO on the variability of the Asian-Australian monsoons as simulated in GCM experiments, *J. Climate*, *13*, 4287–4309, 2000.

Li, C., and M. Yanai, The onset and interannual variability of the Asian summer monsoon in relation to land-sea thermal contrast, *J. Climate*, *9*, 358–375, 1996.

Parthasarathy, B., A. A. Munot, and D. R. Kothawale, All India monthly and seasonal rainfall series: 1871-1993, *Theor. Appl. Climatol.*, *49*, 217–224, 1994.

Rodwell, M. J., and B. J. Hoskins, Monsoons and dynamics of deserts, *Quart. J. Roy. Meteor. Soc.*, *122*, 1385–1405, 1996.

Schneider, E., and R. Lindzen, Axially symmetric steady state models of the basic state of instability and climate studies. Part I: Linearized calculations, *J. Atmos. Sci.*, *34*, 23–279, 1977.

Soman, M., and K. KrishnaKumar, Space-Time evolution of Meteorological features associated with the onset of Indian summer monsoon, *Mon. Wea. Rev.*, *121*, 1177–1194, 1993.

Tomas, R., and P. Webster, The role of inertial instability in determining the location and strength of near-equatorial convection, *Quart. J. Roy. Meteor. Soc.*, *123*, 1445–1482, 1997.

Uppala, S. M., P. Kallberg, A. Simmons, and co authors, The ERA-40 Reanalysis, *Quart. J. Roy. Meteor. Soc.*, p. submitted, 2004.

Webster, P. J., V. O. Magana, T. N. Palmer, J. Shukla, R. T. Tomas, M. Yanai, and T. Yasunari, Monsoons: Processes, predictability and the prospects of prediction, *J. Geophys. Res.*, *103(C7)*, 14,451–14,510, 1998.

Yanai, M., C. F. Li, and Z. S. Song, Seasonal heating of the Tibetan Plateau and its effects on the evolution of the Asian Summer Monsoon, *J. Meteor. Soc. Japan*, *70*, 319–351, 1992.

B. N. Goswami, Prince K. Xavier Centre for Atmospheric and Oceanic Sciences, Indian Institute of Science, Bangalore, 560012, INDIA. (goswamy@caos.iisc.ernet.in, xavier@caos.iisc.ernet.in)

(Received _____.)

Table 1: (Supplementary) Correlations between OD, WD, LRS, EIMR during JJAS and EIMR during LRS from NC, and OD, WD and LRS from ERA, with monthly anomalies of Niño4 SST.

	NC					ERA		
	OD	WD	LRS	EIMR (JJAS)	EIMR (LRS)	OD	WD	LRS
Jan	0.0100	-0.3277	-0.2264	0.0000	0.0000	0.1572	-0.2145	-0.2387
Feb	0.3426	-0.0462	-0.2390	0.2263	0.0090	0.2818	0.0267	-0.1512
Mar	0.3846	-0.0850	-0.2906	0.1270	-0.0795	0.3286	-0.0094	-0.2036
Apr	0.4125	-0.1809	-0.3721	0.1041	-0.1387	0.4216	-0.1092	-0.3265
May	0.4743	-0.3066	-0.4941	0.0332	-0.2526	0.4561	-0.2341	-0.4313
Jun	0.4174	-0.3500	-0.4887	0.0560	-0.2202	0.4057	-0.2885	-0.4377
Jul	0.4679	-0.4976	-0.6187	-0.0489	-0.3664	0.4474	-0.4470	-0.5693
Aug	0.4403	-0.5850	-0.6606	-0.1164	-0.4320	0.3793	-0.5419	-0.5924
Sep	0.2971	-0.6079	-0.5891	-0.1109	-0.3829	0.2870	-0.5507	-0.5429
Oct	0.2471	-0.6620	-0.5952	-0.1043	-0.3699	0.2700	-0.6089	-0.5718
Nov	0.2062	-0.6110	-0.5360	-0.1222	-0.3619	0.2275	-0.5904	-0.5339
Dec	0.2597	-0.6147	-0.5711	-0.1310	-0.3886	0.2699	-0.5859	-0.5563

Table 2: (Supplementary) OD, WD and LRS from NCEP and ERA in Julian days.

	NCEP			ERA		
	OD	WD	LRS	OD	WD	LRS
1950	144	287	143			
1951	154	275	121			
1952	142	278	136			
1953	155	279	124			
1954	146	284	138			
1955	146	282	136			
1956	133	289	156			
1957	152	276	124			
1958	153	283	130	152	283	131
1959	146	288	142	145	291	146
1960	140	287	147	138	289	151
1961	146	288	142	130	289	159
1962	146	274	128	142	274	132
1963	149	277	128	148	276	128
1964	155	288	133	137	289	152
1965	147	270	123	144	270	126
1966	148	267	119	147	266	119
1967	140	276	136	140	278	138
1968	156	283	127	155	282	127
1969	147	273	126	137	273	136
1970	147	280	133	142	280	138
1971	149	287	138	144	288	144
1972	162	263	101	147	263	116
1973	148	281	133	146	288	142
1974	148	276	128	145	279	134
1975	146	288	142	145	288	143
1976	147	275	128	144	276	132

Table 3: Continuation of Supplementary Table 2.

	NCEP			ERA		
	OD	WD	LRS	OD	WD	LRS
1977	156	278	122	148	280	132
1978	142	280	138	141	280	139
1979	156	275	119	155	278	123
1980	154	275	121	154	273	119
1981	145	276	131	145	277	132
1982	152	274	122	151	275	124
1983	155	290	135	153	291	138
1984	147	269	122	147	269	122
1985	144	275	131	144	277	133
1986	150	266	116	137	267	130
1987	153	274	121	152	274	122
1988	141	282	141	140	284	144
1989	139	284	145	139	285	146
1990	136	281	145	136	284	148
1991	151	272	121	151	273	122
1992	162	278	116	161	278	117
1993	150	278	128	149	278	129
1994	149	264	115	148	265	117
1995	152	279	127	136	279	143
1996	147	282	135	145	282	137
1997	156	264	108	156	264	108
1998	156	282	126	155	282	127
1999	142	277	135	142	277	135
2000	139	271	132	136	275	139
2001	144	283	139	142	285	143
2002	139	268	129			
Mean	149	278	129	145	279	133
S.D	6.5	7.2	10.6	6.6	7.4	11.1

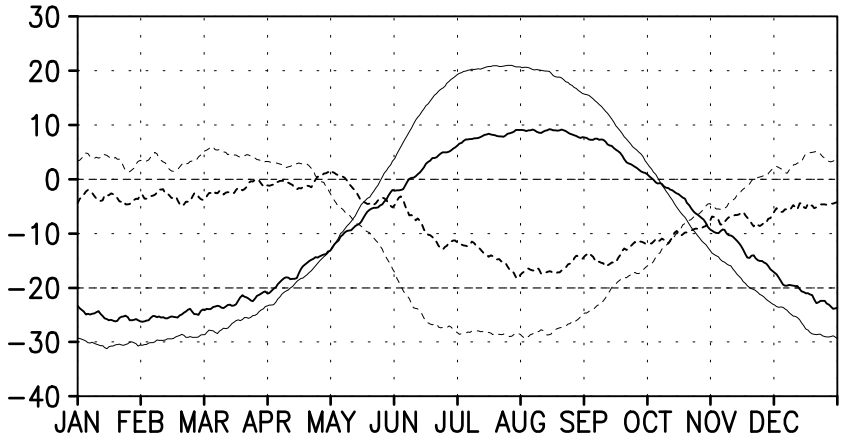

Figure 1: (Supplementary) Evolution of meridional gradient of TT between two boxes similar to those in Fig.1a but over the longitudes between 40°E-110°E and 110°E-150°E respectively (solid lines with increasing thickness). Zonal wind shear between 200 hPa and 850 hPa averaged between Eq.-15°N over the two longitude domains are shown by dotted lines of respective thickness.

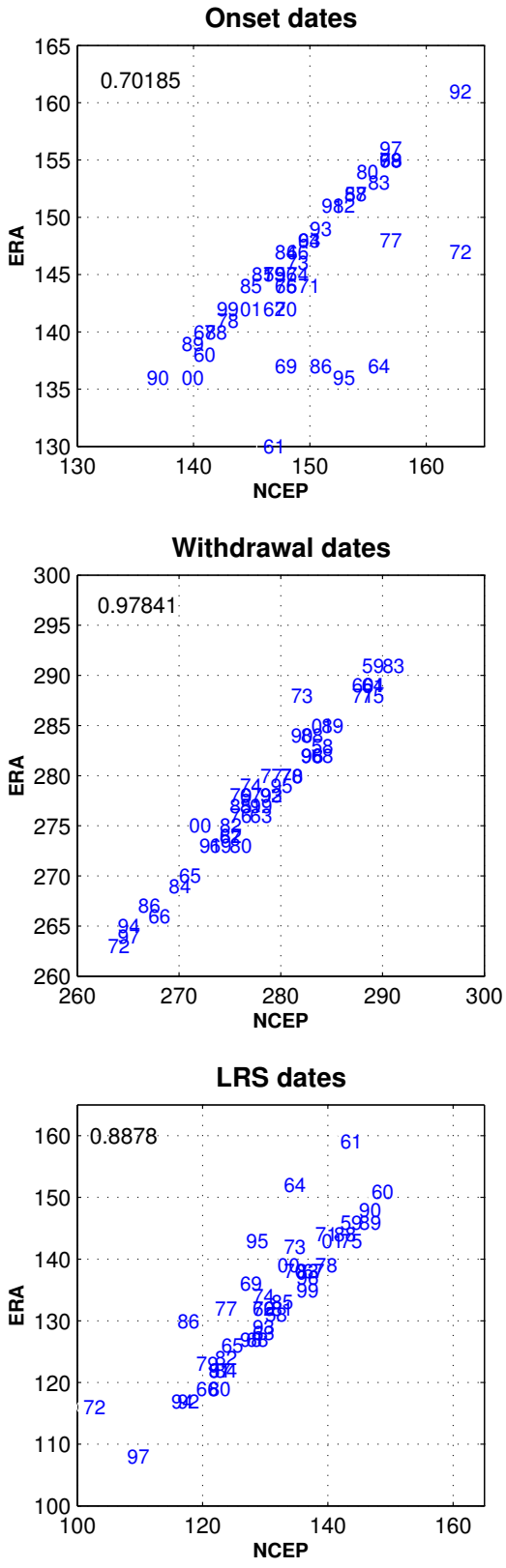

Figure 2: (Supplementary) The scatter plot of OD, WD and LRS dates from ERA and NC from 1958 to 2001. The correlation coefficient between ERA and NC are given in respective panels.

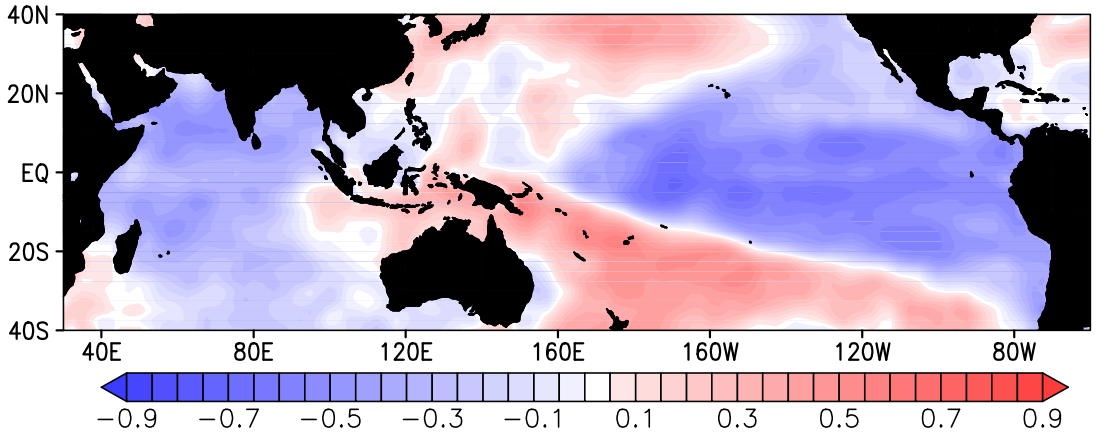

Figure 3: (Supplementary) Correlation coefficient between LRS and June-September SST anomalies, based on data between 1950 and 2003.

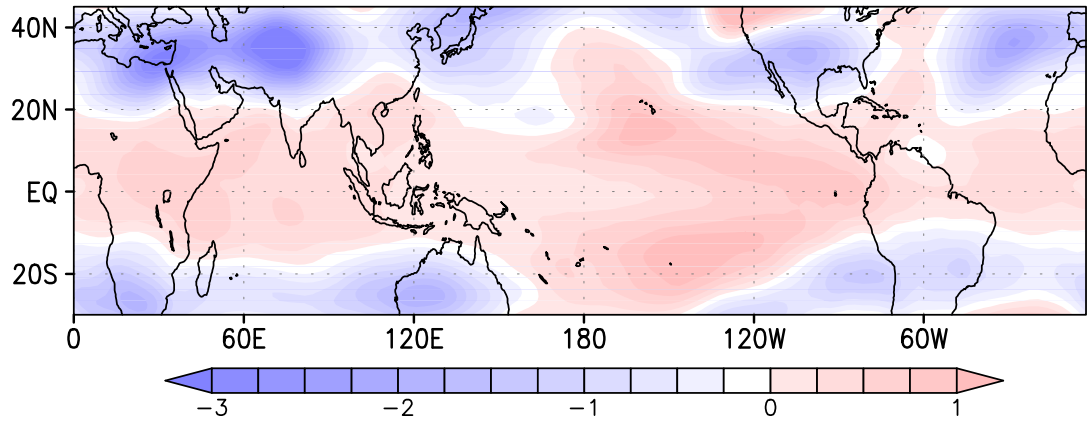

Figure 4: (Supplementary) Tropospheric temperature (TT, averaged between 200 and 700 hPa) response to El Nino SST forcing during the period between 15 May and 15 June. An ensemble of simulations of an Atmospheric General Circulation Model (AGCM, here we use NCAR CCM3) forced by El Nino composite SST were carried out. Integrations were carried out over an entire year (year(0)) of El Nino composites. Another 10 member control simulation is done with climatological SST forcing. The difference of TT between the El Nino composite run and the control run, averaged between 15 May and 15 June is plotted (K).

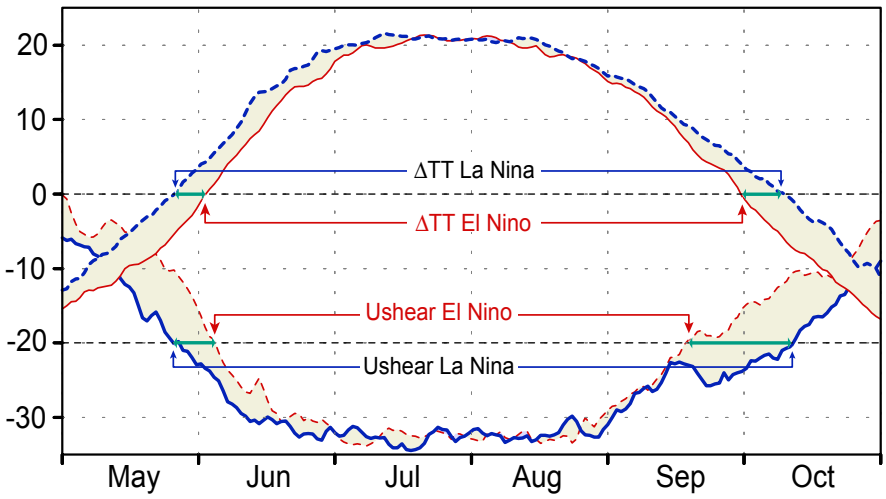

Figure 5: (Supplementary) Average change in onset and withdrawal dates from zero crossings of composite ΔTT (K $\times$ 6) for El Niño (thick dashed) and La Nina (thin solid) together with corresponding composites of vertical shear of zonal winds (thick solid and thin dashed respectively, m s^{-1}).